CO_2 Reduction Selective for $C_{\geq 2}$ Products on Polycrystalline Copper with N-substituted Pyridinium Additives

Zhiji Han,[‡] Ruud Kortlever,[‡] Hsiang-Yun Chen, Jonas C. Peters,* and Theodor Agapie*

Division of Chemistry and Chemical Engineering, California Institute of Technology, Pasadena, California 91125, United States

Supplementary Information

Table of contents

S1. Materials

All reagents were used as received unless otherwise stated. Compounds **1**, **3** and **4**,[1] 1-(2,4-dinitrophenyl)-pyridinium chloride,[2] and 1-(2,4-dinitrophenyl)-4-phenylpyridinium chloride,[3] were synthesized according to published procedures. Compounds **1, 3** and **4** were recrystallized from a mixture of MeOH/Et_2O (1:5) prior to use.

Copper foil (99.999% Cu, 25 mm × 50 mm × 1 mm), phosphoric acid (85%, TraceSelect), potassium carbonate (99.995%), potassium hydroxide (semiconductor grade, 99.99% trace metals basis) and carbon-^{13}C dioxide (99 atom % ^{13}C, <3 atom % ^{18}O), ferrocene carboxylic acid, ≥97.0% trace metal basis), 4-phenylpyridine, 1-chloro-2,4-dinitrobenzene, 4-chloroanaline, *p*-toluidine, *p*-anisidine, 4-*tert*-butylaniline, *N,N*-dimethyl-*p*-phenylenediamine, 1-butylpyridinium chloride, 1-(4-pyridyl)pyridinium chloride hydrochloride, methyl viologen dichloride hydrate, methylene blue, 1,3-bis(2,4,6-trimethylphenyl)imidazolium chloride, pyridine hydrochloride, bis(cyclopentadienyl)cobalt(II), were purchased from Sigma-Aldrich. Carbon rods (99.999% C) were purchased from Strem Chemicals. 1,1'-diphenyl-4.4'-bipyridinium dichloride was purchased from TCI Chemicals.

Water was purified by a Nanopure Analytical Ultrapure Water System (Thermo Scientific) or a Milli-Q Advantage A10 Water Purification System (Millipore) with specific resistance of 18.2 MΩ·cm at 25 °C. Natural abundance carbon dioxide (Research grade) was purchased from Airgas. Deuterium dioxide (D 99.96%), d-chloroform (D 99.8%) and d_2-dichloromethane (D 99.8%) were purchased from Cambridge Isotope Laboratories. ^{1}H and ^{13}C NMR spectra were recorded on a Varian 300 MHz instrument or 100.62 MHz on a Bruker AscendTM 400 MHz spectrometer, with shifts reported relative to the residual solvent peak.

Upon receiving copper foil was polished to a mirror-like finish using alumina pastes (0.05 μm, Buehler) followed by rinsing and sonicating in water to remove residual alumina. Before each experiment, the copper foil was electropolished using a method similar to the one employed by Kuhl *et al*.:[4] In a 85% phosphoric acid bath, +2.1 V versus a carbon rod counter electrode was applied to the Cu foil for 5 minutes and the foil was subsequently washed with ultra-pure water and dried under a stream of nitrogen gas.

Potassium bicarbonate electrolytes ($KHCO_{3(aq)}$, 0.1 M) were prepared by sparging an aqueous solution of potassium carbonate ($K_2CO_{3(aq)}$, 0.05 M) with CO_2 for at least 1 hour prior to electrolysis. Such process converts K_2CO_3 into $KHCO_3$ and saturates the electrolyte solution with CO_2. Pyridinium-derivatives were added to the 0.1 M $KHCO_{3(aq)}$ catholyte whereas 0.1 M $KHCO_{3(aq)}$ without any pyridinium-derivatives was used as the anolyte.

S2. Synthesis

2.1 Synthesis of 1,1'-ditolyl-4.4'-dihydro-4.4'-bipyridine (2)

In a nitrogen glovebox, a solution of bis(cyclopentadienyl)cobalt(II) (202 mg, 1.07 mmol) in CH_2Cl_2 (3 mL) was added to a solution of compound **1** (100 mg, 0.49 mmol) in CH_2Cl_2 (2 mL). The homogenous solution was stirred for 10 min whereafter the solvent was removed under reduced pressure to yield a dark blue solid. The solid was washed with dimethoxyethane (5 x 5 mL) and the light orange product was extracted with benzene (10 mL). Single crystals amenable to X-ray diffraction studies can be grown from diffusion of Et_2O into a CH_2Cl_2 solution. Yield. 40 mg (48%). ^{1}H NMR (300 MHz, CD_2Cl_2, 25 ^{o}C): δ = 2.28 (s, 6 H), 3.11 (m, 2 H), 4.66 (d, 4 H), 6.51 (d, 4 H), 6.90 (d, 4 H), 7.09 (d, 4H). ^{13}C NMR (100 MHz, CD_2Cl_2, 25 ^{o}C): δ = 20.27, 41.25, 102.77, 117.06, 128.19, 129.80, 131.67, 142.07. HRMS (TOF-MS): calcd. for $C_{12}H_{12}N$: 170.0970 $[M/2]^+$; found: 170.0336.

2.2 Synthesis of 1-(*p*-Me_2N)C_6H_4-pyridinium chloride (5)

Into a microwave vial (40 mL) equipped with a magnetic stir bar 1-(2,4-dinitrophenyl)-pyridinium chloride (562 mg, 2.0 mmol), *N,N*-dimethyl-*p*-phenylenediamine (545 mg, 4.0 mmol), and EtOH/H_2O (60/40) binary solvent (10 mL) were successively added. The vial was sealed and the reaction was performed under microwaves at 130 ^{o}C for 35 min. After reaction, the mixture was concentrated under vacuum. The dark green solid was washed with hexane (3 x 20 mL), then diethyl ether (3 x 20 mL). Product was extracted with water (2 x 5 mL) and dried under vacuum. Recrystallization of this material from a mixture of MeOH/Et_2O (1:5) at -20 ^{o}C over 20 h gave orange brown needles. Yield. 0.25 g (53%). ^{1}H NMR (300 MHz, D_2O, 25 ^{o}C): δ = 2.98 (s, 6 H), 6.98 (m, 2 H), 7.55 (m, 2 H), 8.12 (t, 2 H), 8.57 (t, 1 H), 8.93 (d, 2 H). ^{13}C NMR (100 MHz, D_2O, 25 ^{o}C): δ = 39.87, 113.56, 124.49, 127.95, 132.28, 143.49, 144.92, 152.46. HRMS (TOF-MS): calcd. for $C_{13}H_{15}N_2$: 199.1235 $[M]^+$; found: 199.1226.

2.3 Synthesis of 1-(*p*-*t*Bu)C_6H_4-pyridinium chloride (6)

Into a microwave vial (40 mL) equipped with a magnetic stir bar 1-(2,4-dinitrophenyl)-pyridinium chloride (562 mg, 2.0 mmol), 4-*tert*-butylaniline (596 mg, 4.0 mmol), and EtOH/H_2O (60/40) binary solvent (10 mL) were successively added. The vial was sealed and the reaction was performed under microwaves at 130 ^{o}C for 35 min. After reaction, the mixture was concentrated under vacuum. The red solid was purified by flush column chromatography (silica; MeCN to MeOH). Recrystallization of MeOH fraction from a mixture of MeOH/Et_2O (1:5) at -20 ^{o}C gave colorless needles. Yield. 0.34 g (62%). ^{1}H NMR (300 MHz, D_2O, 25 ^{o}C): δ = 1.33 (s, 9 H, *t*-Bu), 7.64-7.79 (m, 4 H), 7.45 (d, 1 H),

8.24 (t, 2 H), 8.74 (t, 1 H), 9.05 (d, 2 H). ^{13}C NMR (100 MHz, D_2O, 25 ^{o}C): δ = 29.48, 33.50, 122.63, 126.72, 127.43, 139.27,143.14, 145.49, 154.48. HRMS (TOF-MS): calcd. for $C_{15}H_{18}N$: 212.1439 $[M]^+$; found: 212.1432.

2.4 Synthesis of 1-(*p*-Me)C_6H_4-4-phenylpyridinium chloride (7)

Into a microwave vial (40 mL) equipped with a magnetic stir bar 1-(2,4-dinitrophenyl)-4-phenylpyridinium chloride (717 mg, 2.0 mmol), *p*-toluidine (257 mg, 2.4 mmol), and EtOH/H_2O (60/40) binary solvent (10 mL) were successively added. The vial was sealed and the reaction was performed under microwaves at 130 ^{o}C for 35 min. After reaction, the mixture was concentrated under vacuum. The crude product was stirred in MeCN (10 mL) for 1 h and filtered. The filtrate was concentrated under vacuum. Recrystallization of this material from a mixture of MeCN/Et_2O (1:5) at room temperature gave colorless needles. Yield. 0.35 g (62%). ^{1}H NMR (300 MHz, D_2O, 25 ^{o}C): δ = 2.45 (s, 3 H), 7.52-7.66 (m, 7 H), 7.98 (m, 2 H), 8.37 (d, 2 H), 8.96 (d, 2 H). ^{13}C NMR (100 MHz, D_2O, 25 ^{o}C): δ = 20.21, 123.38, 124.66, 128.02, 129.71, 130.84, 132.46, 133.36, 139.70, 142.33, 143.58, 156.75. HRMS (TOF-MS): calcd. for $C_{18}H_{16}N$: 246.1283 $[M]^+$; found: 246.1285.

2.5 Synthesis of 1-(*p*-Me)C_6H_4-pyridinium-d5 chloride

This compound was synthesized following the same procedure as compound **1**.[1] Pyridine-d5 was used to synthesize the 1-(2,4-dinitrophenyl)-pyridinium-d5 chloride at 95% yield. 1-(*p*-Me)C_6H_4-pyridinium-d5 was isolated at 58% yield. HRMS (TOF-MS): calcd. for $C_{12}H_7D_5N$: 175.1292 $[M]^+$; found: 175.1284.

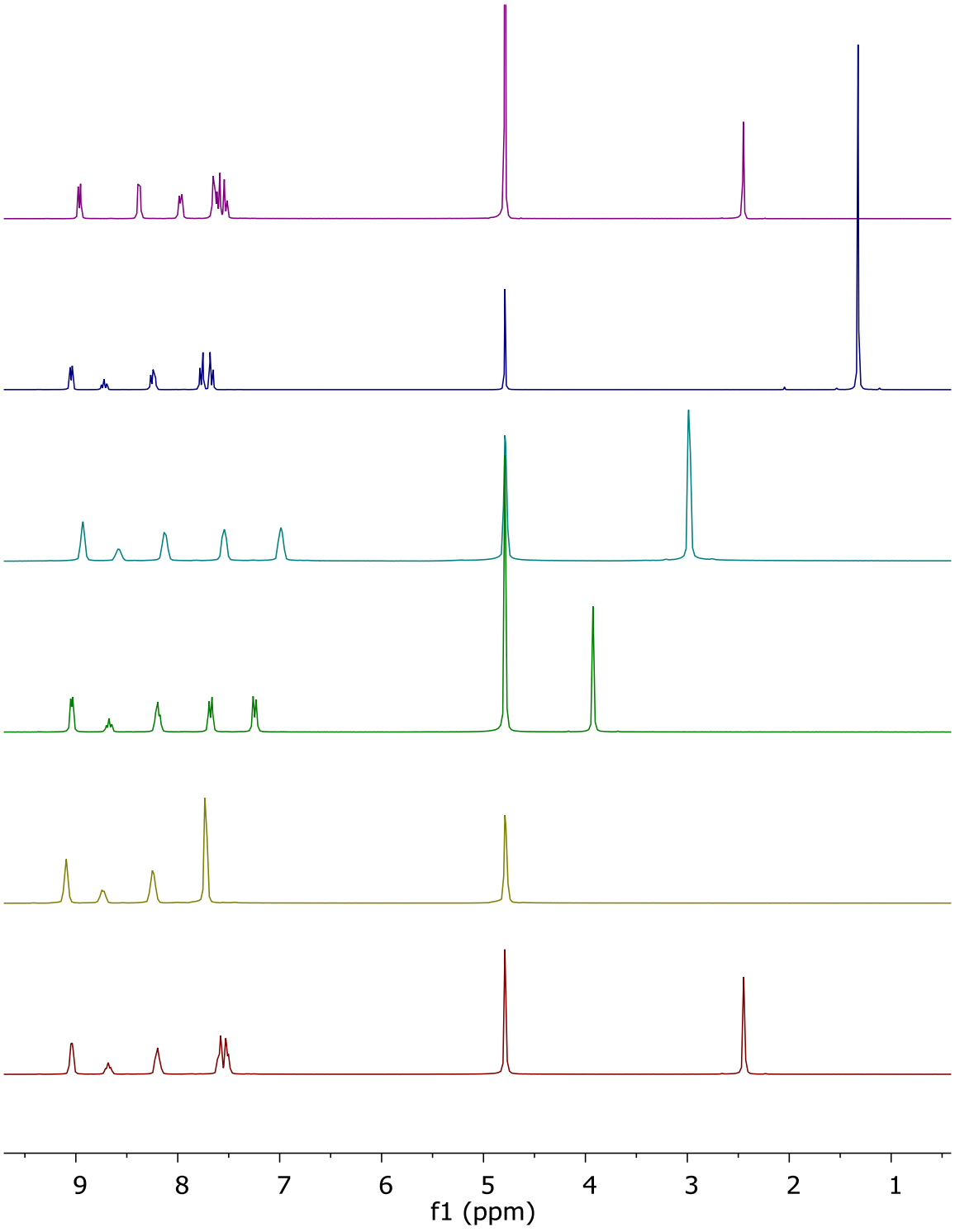

Figure S1. ^{1}H NMR (300 MHz) spectra of compounds **1**, **3**, **4**, **5**, **6**, and **7** (from bottom to top) in D_2O.

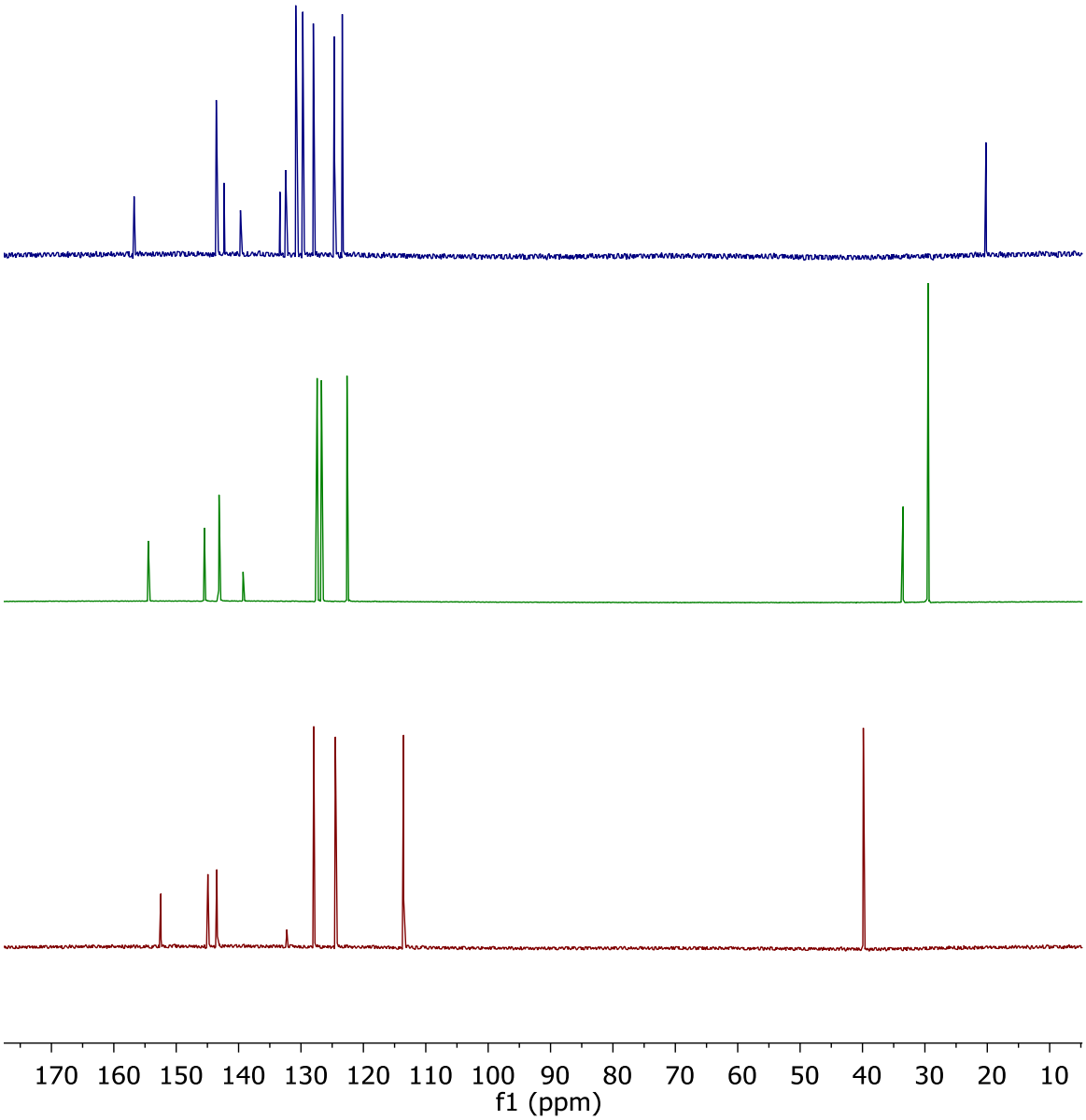

Figure S2. ^{13}C NMR (100 MHz) spectra of compounds **5**-**7** (from bottom to top) in D_2O.

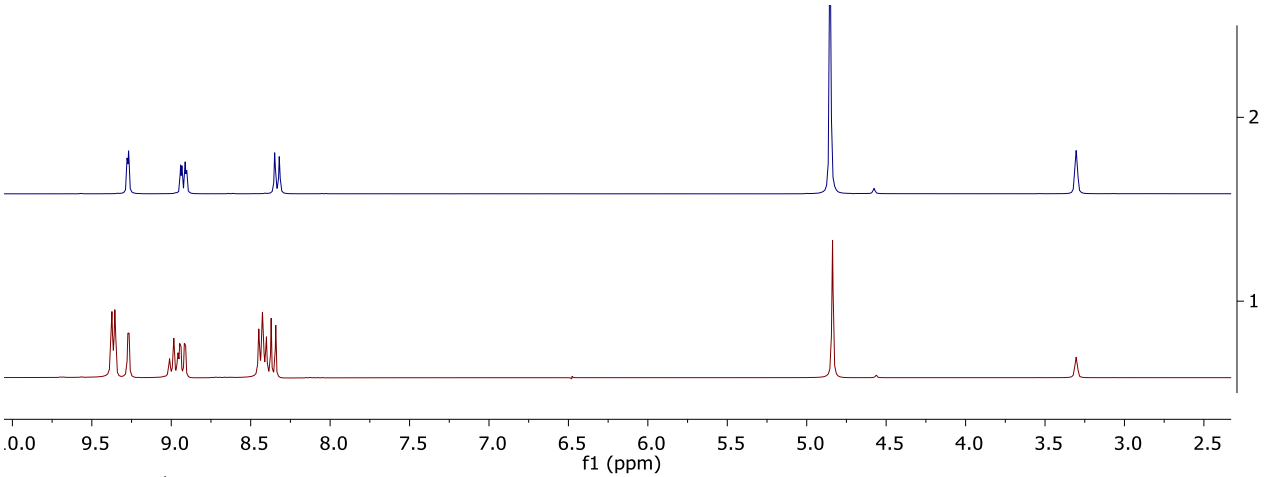

Figure S3. ^{1}H NMR (300 MHz) spectra of 1-(2,4-dinitrophenyl)-pyridinium (red) and 1-(2,4-dinitrophenyl)-pyridinium-d5 (blue) in CD_3OD.

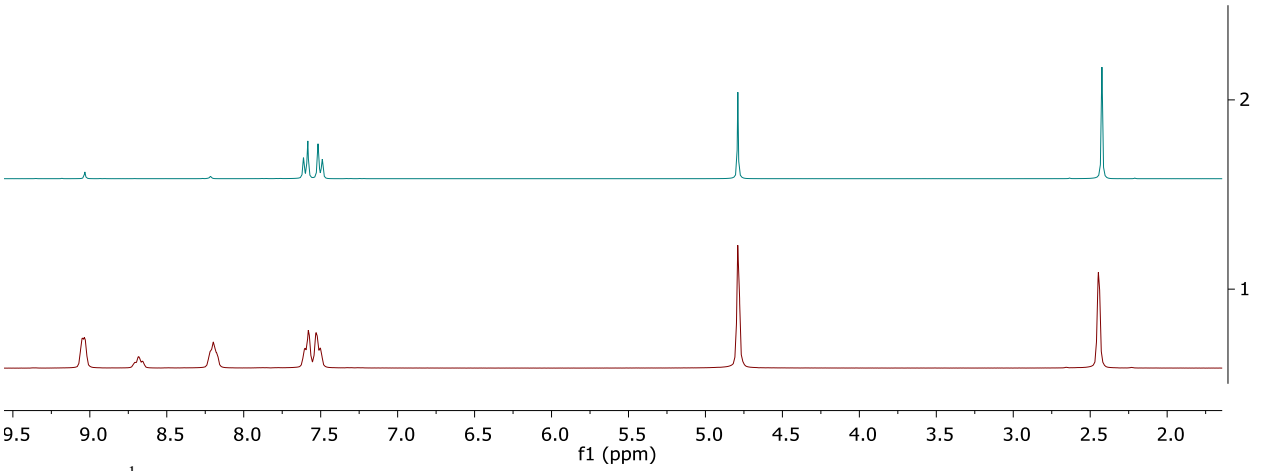

Figure S4. ^{1}H NMR (300 MHz) spectra of **1** (red) and **1-d5** (green) in D_2O

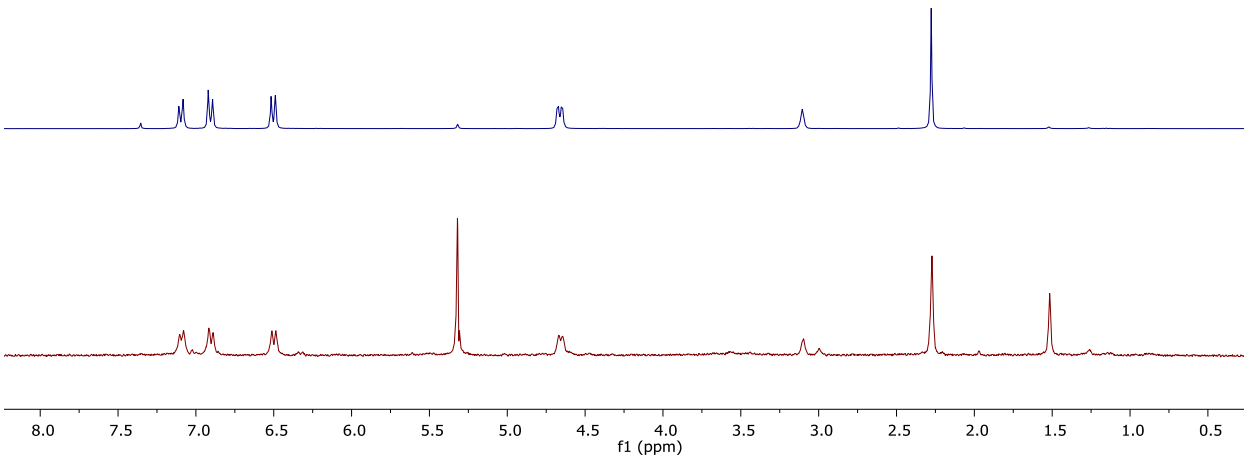

Figure S5. ^{1}H NMR (300 MHz) spectra of the surface material on Cu electrode after electrolysis in the presence of **1** (red) and 1,1'-ditolyl-4.4'-dihydro-4.4'-bipyridine (**2**) (blue) in CD_2Cl_2.

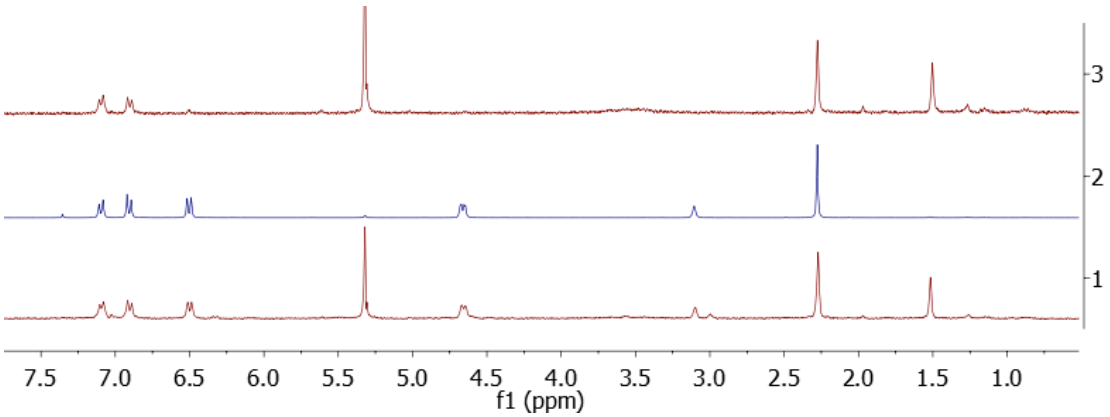

Figure S6. ^{1}H NMR (300 MHz) spectra of the surface material on Cu electrode after electrolysis in the presence of **1** (bottom), 1,1'-ditolyl-4.4'-dihydro-4.4'-bipyridine (**2**), (middle) and the surface material on Cu electrode after electrolysis in the presence of **1-d$_5$** (top) in CD_2Cl_2.

S3. Electrochemical measurements

Chronoamperometry measurements were carried out in a custom-made PEEK flow cell setup similar to the one reported by Ager *et al.*,[5] using a copper foil as working electrode and a platinum foil as counter electrode. The cathode compartment was separated from the anode compartment by a Selemion AMV anion-exchange membrane (AGC Engineering Co.). All potentials were measured versus a leakless Ag/AgCl reference electrode (Innovative Instruments) with an outer diameter of 1 mm that was inserted into the cathode compartment. The reference electrode was calibrated against ferrocene carboxylic acid in a 0.2 M phosphate buffer solution at pH 7.0 (+0.239 V vs. Ag/AgCl).

Electrochemical impedance measurements were carried out prior to electrolysis experiments to determine the Ohmic resistance of the flow cell. The impedance measurements were carried out using a Biologic VMP3 multichannel potentiostat, at frequencies ranging from 200 kHz to 100 MHz to measure the solution resistance. Since the resistance of the cell can vary for each experiment, it is important to correct for the resistance of the cell so that the applied potential during the electrolysis experiment corresponds to the intended electrode potential. A Nyquist plot was plotted and in the high-frequency part a linear fit was performed and the axis intersection was calculated. The value of this intersection represents the Ohmic resistance of the cell. An average of 3 measurements was taken to calculate the value of R. Typically, small resistances were measured, ranging from 50 to 60 Ω. The potentiostat was set to compensate for 85 % of the Ohmic drop during the electrolysis experiments, with the remaining 15 % being compensated for after the measurements.

Cyclic Voltammetry (CV) measurements were recorded at 25 ^{o}C on a Pine Instrument Company AFCBP1 bipotentiostat using a one-compartment cell with a Cu disk working electrode (diameter 3 mm), Pt counter electrode, and a Ag/AgCl reference electrode. Data were recorded using the Pine Instrument Company AfterMath software package. The electrolyte solutions were either CO_2 or N_2 saturated 0.1 M $KHCO_3$ in H_2O.

Electrochemical measurements were recorded using a Biologic VMP3 multichannel potentiostat. All potentials were converted from the Ag/AgCl scale to the reversible hydrogen electrode (RHE) scale by using $V_{RHE} = V_{meas} + 0.197 + 0.059 \times pH$, where V_{RHE}, V_{meas} and pH are potential vs RHE, (measured) potential vs Ag/AgCl reference electrode and pH of the electrolyte (6.8), respectively. Prior to electrolysis the solution resistance was measured with electrochemical impedance spectroscopy (EIS) as mentioned earlier.

During electrolysis, the effluent gas stream coming from the flow cell (5 ml/min) was flowed into the sample loops of a gas chromatograph (GC-FID/TCD, SRI 8610C, in Multi Gas 5 configuration) equipped with HayesepD and Molsieve 5A columns. Methane, ethylene, ethane, carbon monoxide were detected by a methanizer-flame ionization detector (FID) and the hydrogen was detected by a thermal conductivity detector (TCD). 2 mL of gas was sampled every 15 minutes to determine the concentration of gaseous products. After electrolysis, the liquid products in both catholytes and anolytes were quantified by both HPLC (Thermo Scientific Ultimate 3000) and ^{1}H NMR. For ^{1}H NMR, solutions containing 90% electrolyte and 10% D_2O (v/v) with internal standard (N,N-dimethylformamide or dimethylsulfoxide) were prepared and measured using a water suppression technique on a Bruker 400 MHz NMR spectrometer.

For isotope labeling experiments the same experimental configurations as described above were employed except $KH^{13}CO_{3(aq)}$ solution and $^{13}CO_2$ were used as the electrolyte and CO_2 source, respectively. To prepare the 0.1 M $KH^{13}CO_{3(aq)}$ solution, 50 mL of nanopure water was sparged with nitrogen for 1 h and was added to potassium hydroxide (0.32 g containing 12.6% water) in a Schlenk flask under nitrogen atmosphere. The headspace was evacuated for a few seconds, and $^{13}CO_2$ was introduced. The solution was stirred vigorously for 5 h and an aliquot was extracted to make sure the pH was ~7. The solution was then added to a pre-vacuumed 4 mL vial containing **1** to yield the final electrolyte solution of 0.1 M $KH^{13}CO_{3(aq)}$ and 10 mM **1**. During the electrolysis, $^{13}CO_2$ was introduced from the bottom of the flow cell at 5 ml/min. The outlet was connected to the inlet of the sample loop of the GC-FID/TCD for quantitative analyses every 15 min. To collect the gaseous products for GC-MS and NMR analyses, the outlet of the GC sample loops was connected to a syringe with rubber plunger pulled by a syringe pump set to the same rate as the gas flow. GC-MS analyses was performed using an Agilent 7820A GC coupled with a 5977E MS with a heated cold quadrupole detector and a capillary CarbonPLOT column for identification of the mass fragmentation of ethylene.

The background signal was subtracted. To prepare the NMR samples of the collected gas, a 6 inch long NMR tube containing $CDCl_3$ (0.5 mL) was fitted with a rubber septum, cooled in liquid nitrogen, and evacuated through a needle. 5 mL of the collected gas was then injected, and the tube was allowed to warm to room temperature for NMR measurement.

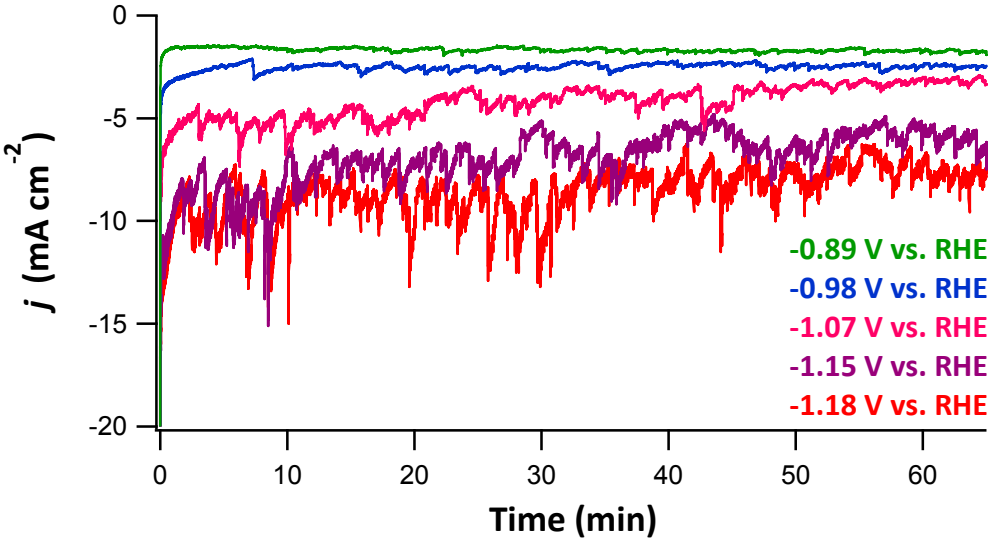

Figure S7. Chronoamperograms of electrolysis using a copper polycrystalline electrode in a CO_2 saturated 0.1 M $KHCO_3$ electrolyte with a flow of 5 mL/min CO_2 at different applied potentials.

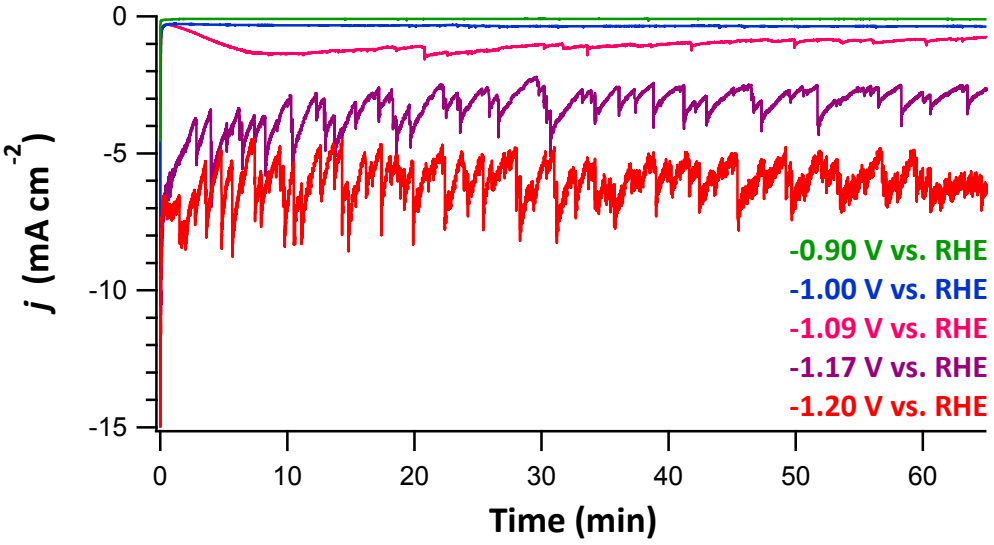

Figure S8. Chronoamperograms of electrolysis using a copper polycrystalline electrode in a CO_2 saturated 0.1 M $KHCO_3$ electrolyte with 10 mM N-tolyl pyridinium (**1**) and a flow of 5 mL/min CO_2 at different applied potentials.

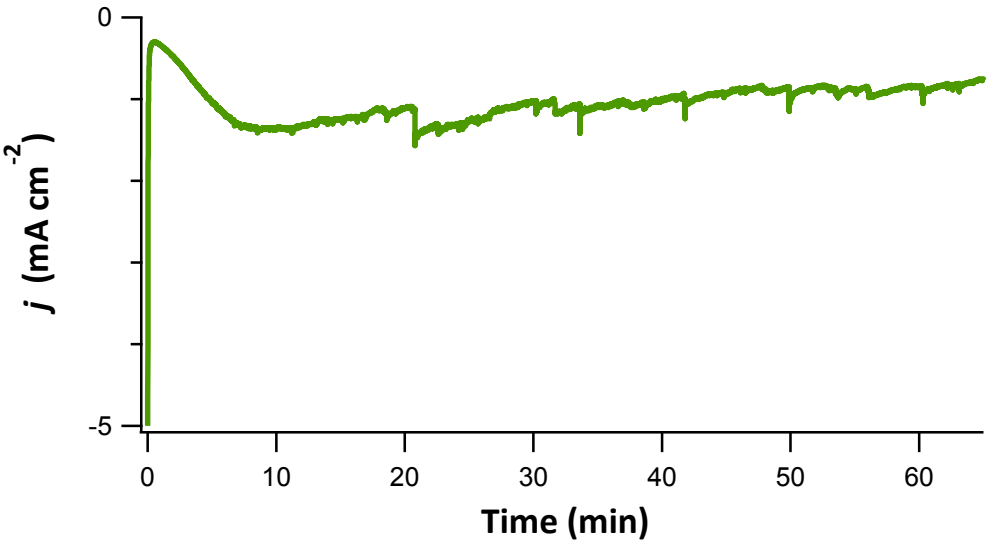

Figure S9. Chronoamperogram of electrolysis at -1.09 V vs. RHE using a copper polycrystalline electrode in a CO_2 saturated 0.1 M $KHCO_3$ electrolyte with 10 mM N-tolyl pyridinium (**1**) and a flow of 5 mL/min CO_2.

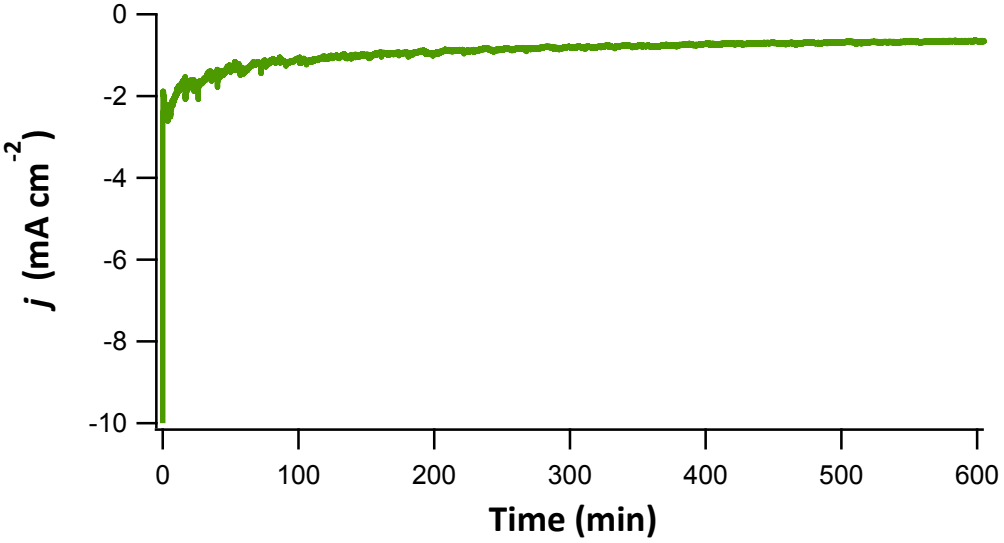

Figure S10. Chronoamperogram of long term electrolysis over the course of 10 hours at -1.09 V vs. RHE using a copper polycrystalline electrode in a CO_2 saturated 0.1 M $KHCO_3$ electrolyte with 10 mM N-tolyl pyridinium (**1**) and a flow of 5 mL/min CO_2.

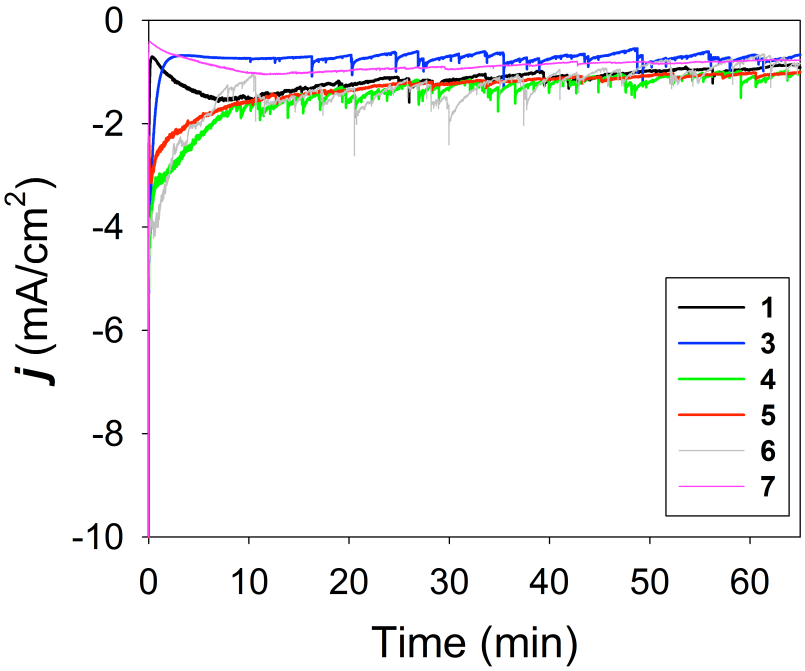

Figure S11. Chronoamperograms of electrolysis with 10 mM of compounds **1**, **3**, **4**, **5**, **6**, and **7** using a copper polycrystalline electrode in a CO_2 saturated 0.1 M $KHCO_3$ electrolyte with a flow of 5 mL/min CO_2 at an applied potential of -1.1 V vs. RHE.

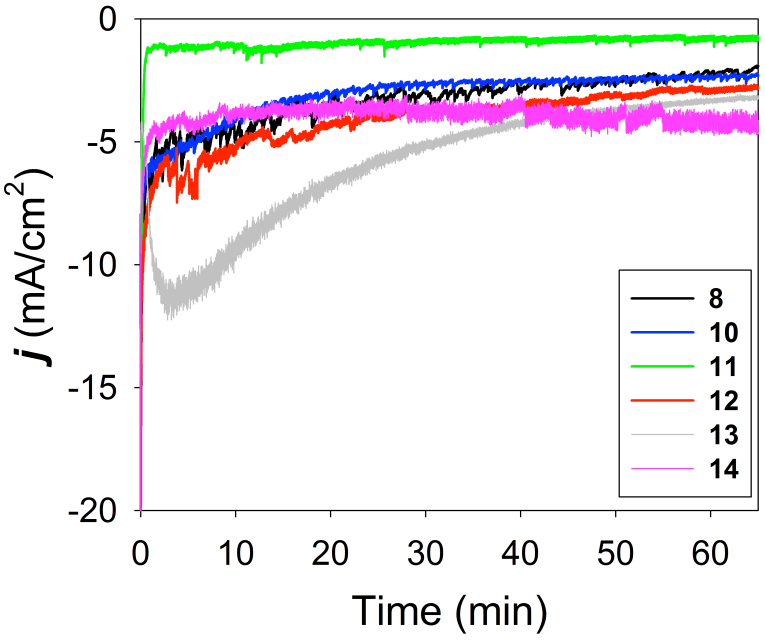

Figure S12. Chronoamperograms of electrolysis with 10 mM of compounds **8**, **10-14** using a copper polycrystalline electrode in a CO_2 saturated 0.1 M $KHCO_3$ electrolyte with a flow of 5 mL/min CO_2.

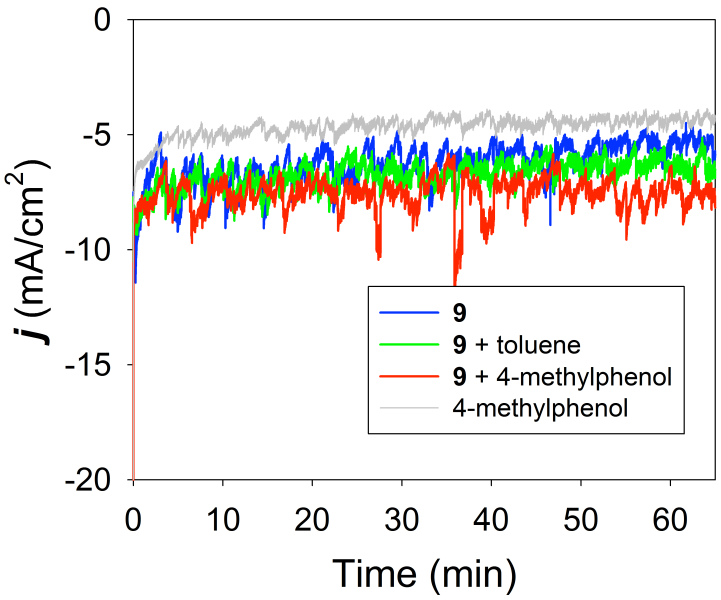

Figure S13. Chronoamperograms of electrolysis on a copper polycrystalline electrode in a CO_2 saturated 0.1 M $KHCO_3$ electrolyte with 10 mM of compounds **9** (blue); 10 mM **9** with saturated toluene (green); 10 mM **9** with saturated 4-methylphenol (red) and saturated 4-methylphenol.

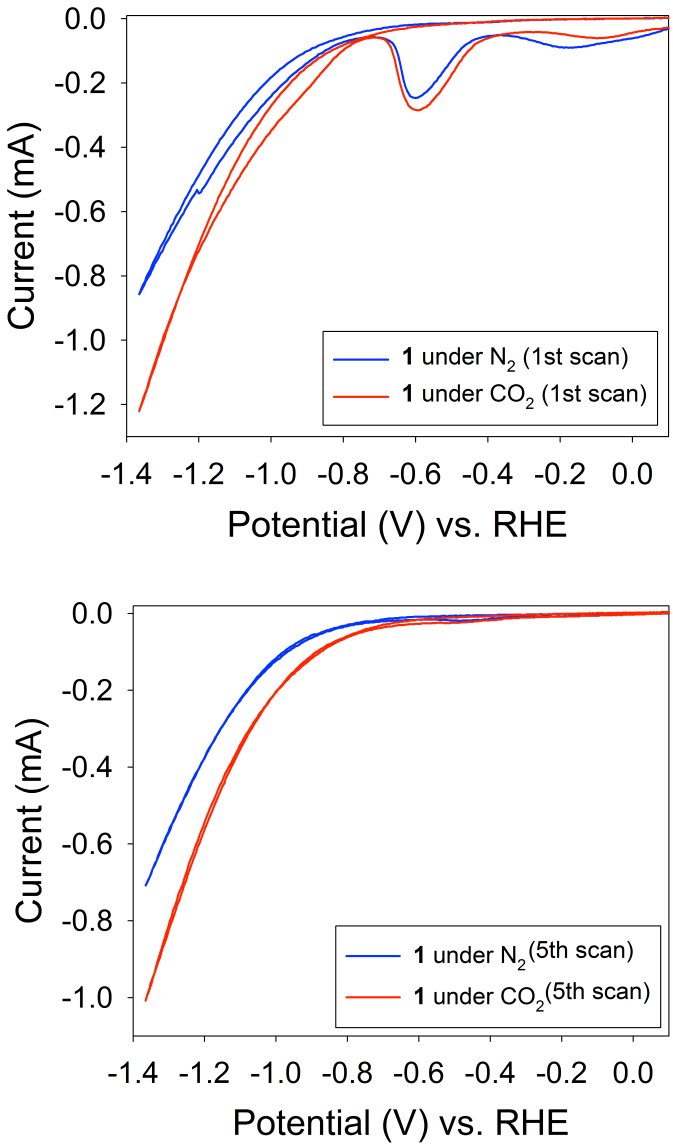

Figure S14. The first scan (top) and fifth scan (bottom) of cyclic voltammograms of 10 mM **1** under N_2 and CO_2 with a Cu disk working electrode in 0.1 M $KHCO_3$ electrolyte at a scan rate of 100 mV/s.

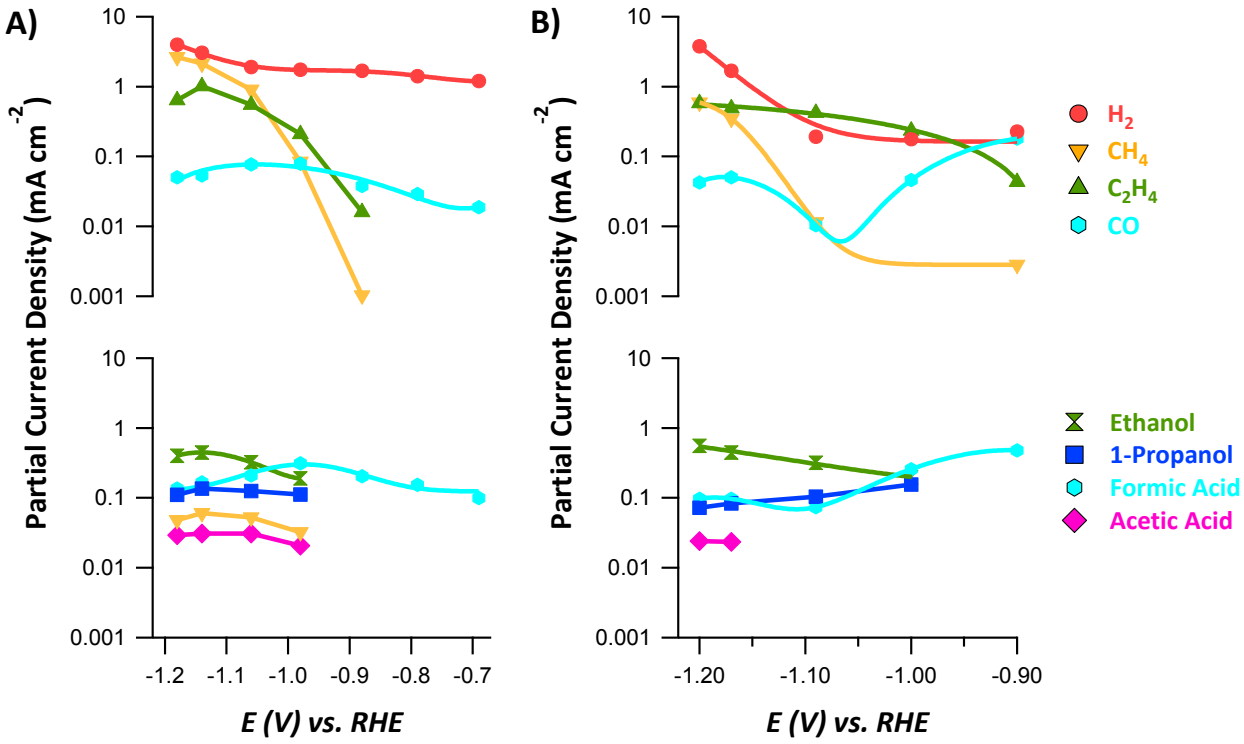

Figure S15. Partial current densities of the major and intermediate products formed during electrochemical CO_2 reduction on a polycrystalline copper electrode in a CO_2 saturated 0.1 M $KHCO_3$ electrolyte (**A)** and during electrochemical CO_2 reduction on a polycrystalline copper electrode in a CO_2 saturated 0.1 M $KHCO_3$ electrolyte with 10 mM N-tolyl pyridinium (**B**).

S4. HPLC analysis for liquid products

Quantitative analysis of the liquid products formed during electrolysis was performed with both high pressure liquid chromatography (HPLC) and ^{1}H NMR. After electrolysis, aliquots of the catholyte were collected and analyzed with HPLC (Thermo Scientific Ultimate 3000). Sample vials were placed in a chilled autosampler and 10 µl of each sample was injected onto the column. Two Aminex HPX 87-H columns (Biorad) placed in series were used to obtain satisfactory product separation. During analysis the column oven was maintained at a steady temperature of 60 ^{o}C, with a steady flow rate of 0.600 mL/min of 1 mM H_2SO_4 aqueous solution as eluent. The effluent stream coming from the column was passed through a refractive index detector (RID) for product detection. A standard calibration curve was used to calculate the initial concentration of each detected product in the sample.

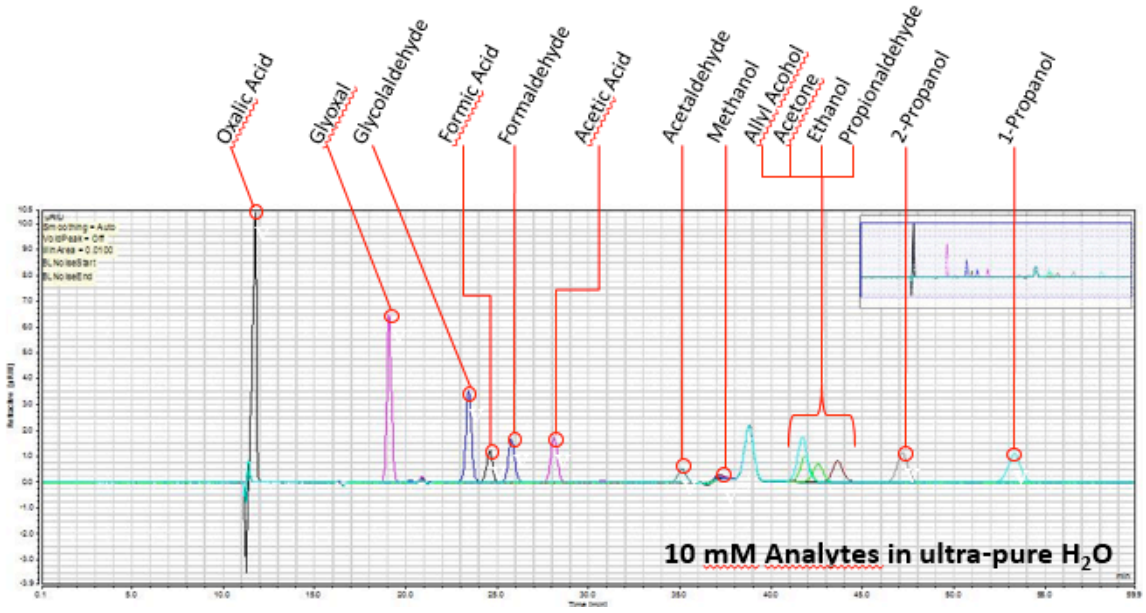

Figure S16. HPLC chromatogram showing an overlay of different analytes at a 10 mM concentration in ultra-pure water.

S5. NMR spectroscopy identification of products

Liquid products formed during electrolysis were identified with ^{1}H-NMR next to the previously mentioned HPLC procedure. After electrolysis samples were taken from the catholyte. For ^{1}H-NMR, 30 µl internal standard solution, consisting of 10 mM DMSO and 50 mM phenol in water, and 70 µl D_2O was added to 0.63 ml electrolyte. The NMR experiments were performed on a Bruker 400 MHz NMR spectrometer, using a presaturation sequence to suppress the water signal.

Table S1. Chemical shifts and assignments of peaks from different (possible) CO_2 reduction products observed in ^{1}H-NMR spectra. The highlighted entries represent the peaks used for calibration and calculation of the product concentration in the electrolyte. The ethanol and methanol peaks were used as reference.

NMR Values			Assignment	
Chemical Shift	1H Splitting	J coupling	Probed Nucleus	Name
9.68	t	1.28	CH_3CH_2CHO	Propionaldehyde
9.66	q	3.00	CH_3CHO	Acetaldehyde
9.60	s		CH_2O	Formaldehyde
8.35	s		CHOOH	Formic acid
7.31	t		Phenol	Internal Standard
6.97	t		Phenol	Internal Standard
6.90	d		Phenol	Internal Standard
5.99	m		CH_2CHCH_2OH	Allyl alcohol
5.28	d	1.68	CH_2CHCH_2OH	Allyl Alcohol
5.23	q	5.20	$CH_3CH(OH)_2$	Acetaldehyde
5.04	t	5.12	$(OH)_2CHCH_2OH$	Glycolaldehyde
4.95	t	5.44	$CH_3CH_2CH(OH)_2$	Propionaldehyde
4.12	d	7.16	CH_2CHCH_2OH	Allyl alcohol
4.10	q	1.64	$CH_3COOCH_2CH_3$	Ethyl acetate
3.65	s		$OHCH_2CH_2OH$	Ethylene glycol
3.64	q	7.08	CH_3CH_2OH	Ethanol
3.54	t	6.64	CH_3CH_2CHOH	n-Propanol
3.50	d	5.12	$(OH)_2CHCH_2OH$	Glycolaldehyde
3.34	s		CH_3OH	Methanol
2.71	s		DMSO	Internal Standard
2.55	q	6.00	CH_3CH_2CHO	Propionaldehyde
2.22	d	3.00	CH_3CHO	Acetaldehyde
2.21	s		CH_3COCH_3	Acetone
2.06	s		$CH_3COOCH_2CH_3$	Ethyl acetate
1.60	dt	5.56	$CH_3CH_2CH(OH)_2$	Propionaldehyde
1.53	sextet	7.40	$CH_3CH_2CH_2OH$	n-Propanol
1.31	d	5.20	$CH_3CH_2(OH)_2$	Acetaldehyde
1.20	t	7.16	CH_3CH_2OH	Ethanol
1.03	t	7.23	CH_3CH_2CHO	Propionaldehyde
0.89	t	7.52	$CH_3CH_2CH(OH)_2$	Propionaldehyde
0.88	t	7.84	$CH_3CH_2CH_2OH$	n-Propanol

S6. Gaseous product analysis

Quantitative Faradaic efficiency measurements of the gas products were carried out using Gas Chromatography (GC). At atmospheric pressure, CO_2 was continuously purged through a two-compartment flow cell at a rate of 5 mL/min while a constant potential was applied for 65 minutes. The cell effluent was sampled via GC once every 15 minutes. CO, CO_2, H_2, methane and ethylene were simultaneously separated using two columns in series (Hayesep D and Molsieve 5A). The quantitative analysis of the gas products was performed using a thermal conductivity detector (TCD) and flame ionization detector (FID). The Faradaic efficiency of the gaseous products was then calculated using the equations:

$$F_m = pF_v/RT, \tag{1}$$

$$\eta_i = \frac{n_i F x_i F_m}{I} \tag{2}$$

where F_m is the molar flow, defined by the pressure p, the volume flow F_v, the gas constant R and temperature T, and where η_i is the Faradaic efficiency of product i, defined by the electron transfer coefficient of the product n_i, Faraday's constant F, the fraction of the product x_i, the molar flow F_m, and the current I.

S7. Additional Faradaic efficiency data

Faradaic efficiency data was calculated from the product concentrations detected by high pressure liquid chromatography (HPLC) and ^{1}H NMR, for liquid products, and gas chromatography (GC), for gaseous products. The reported data is an average of multiple measurements.

Table S2. Faradaic efficiencies (%) of products formed during CO_2 reduction on polycrystalline Cu in 0.1 M $KHCO_3$ at different potentials.

	Faradaic Efficiency (%)														
V_{RHE}	H_2	CH_4	C_2H_4	CO	Formate	Glyoxal	Acetic acid	Allyl Alcohol	Ethanol	1-Propanol	Glycolaldehyde	Methanol	Acetone	Acetaldehyde	Total
-0.69	86.8			1.4	7.2										94.6
-0.79	84.5	0.0		1.7	9.2										94.7
-0.88	78.1	0.0	0.7	1.8	9.5										89.2
-0.98	61.2	3.0	7.3	2.8	11.0		0.7	1.1	6.7	3.9	0.6	0.3	0.8	1.5	100.0
-1.06	42.8	20.2	12.4	1.7	4.7	0.5	0.7	1.2	7.2	2.8	0.4	0.2	0.5	1.0	96.4
-1.14	42.6	29.8	14.2	0.7	2.3	0.2	0.4	0.8	6.2	1.9	0.3	0.1	0.3	0.7	100.8
-1.18	48.3	32.1	7.7	0.6	1.6	0.2	0.4	0.6	4.8	1.3	0.3	0.1	0.3	0.6	99.0

Table S3. Faradaic efficiencies (%) of products formed during CO_2 reduction on Cu in 0.1 M $KHCO_3$ with 10 mM N-tolyl pyridinium at different potentials.

		Faradaic Efficiency (%)								
V_{RHE}	j (mA/cm^2)	H_2	CH_4	C_2H_4	CO	Formate	Acetic acid	Ethanol	1-Propanol	Total
-0.90	-0.94	24.2	0.3	4.6	19.1	50.8				98.1
-1.00	-1.00	17.7	0.0	23.6	4.6	25.8		19.7	15.5	106.0
-1.09	-1.04	18.5	1.1	40.7	1.0	7.1		30.5	10.0	107.8
-1.17	-3.35	50.1	10.4	14.7	1.5	2.9	0.7	13.3	2.5	94.9
-1.20	-6.05	62.5	9.8	9.6	0.7	1.6	0.4	9.2	1.2	93.8

Table S4. Faradaic efficiencies (%) of products formed during CO_2 reduction on Cu in 0.1 M $KHCO_3$ for 65 min each with 10 mM **1** added in various order.

Entry	E_{RHE}	**1** (mM)	j (mA/cm^2)	H_2	CH_4	C_2H_4	CO	Formate	Ethanol	1-Propanol	Total
1	-1.09	10	-0.93	17.7	0.6	41.0	3.6	6.2	28.3	4.3	102
2[a]	-1.09	0	-1.81	25.1	2.5	37.9	3.5	1.8	22.2	2.2	98
3[b]	-1.09	10	-1.11	33.0	2.9	35.3	3.0	5.6	22.8	2.7	107
4[c]	-1.09	0; 10	-1.036	35.6	0.8	28.6	2.6	11.0	16.2	4.6	102

[a]After experiment in entry 1, electrolyte was replaced with 0.1 M $KHCO_{3(aq)}$.
[b]After experiment in entry 2, electrolyte was replaced with 0.1 M $KHCO_{3(aq)}$ and 10 mM **1**.
[c]Electrolysis in 0.1 M $KHCO_3$(aq) for 1 min then 10 mM **1** was added.

Table S5. Faradaic efficiencies (%) of products formed during CO_2 reduction on Cu in 0.1 M $KHCO_3$ prepared from KOH with 10 mM **1** for 65 min.

E_{RHE}	**1** (mM)	CO_2	j (mA/cm^2)	H_2	CH_4	C_2H_4	CO	Formate	Ethanol	1-Propanol	Total
-1.09	10	Natural abundance	-0.89	18.0	0.9	39.4	4.0	N.D.	28.2	4.9	96.1
-1.09	10	$^{13}CO_2$	-1.26	24.6	0.1	34.5	1.3	0.5	22.4	6.6	90.6

Table S6. Faradaic efficiency (%) towards different products produced during CO_2 reduction on a polycrystalline copper electrode in a CO_2 saturated 0.1 M $KHCO_3$ electrolyte with different concentrations of N-tolyl pyridinium (**1**) at an applied potential of -1.1 V vs. RHE.

	Faradaic Efficiency (%)										
1 (mM)	H_2	CH_4	C_2H_4	CO	FA	Ethanol	1-Propanol	$C_{\geq 2}$	$C_{\geq 2}$ / CH_4	Total	j (mA/cm^2)
0	42.8	20.2	12.4	1.7	4.7	7.2	2.8	22.4	0.6	96.4	-4.46
1	31.8	16.1	24.3	4.5	6.1	13.8	4.2	32.3	1.5	102.6	-2.41
5	18.5	12.6	36.5	2.4	5.7	22.6	6.1	65.2	2.9	105.7	-1.39
10	18.5	1.1	40.7	1.0	7.1	30.5	10.0	80.2	37.0	107.8	-1.02
20	16.2	0.5	37.8	1.1	7.4	29.4	5.8	73.0	75.6	98.2	-0.97

Table S7. Faradaic efficiencies (%) of products formed during CO_2 reduction on Cu in 0.1 M $KHCO_3$ for 65 min each with 10 mM **1** added and removed in various order.

Entry	E_{RHE}	**1** (mM)	j (mA/cm^2)	H_2	CH_4	C_2H_4	CO	Formate	Ethanol	1-Propanol	Total
1	-1.09	10	-1.29	21.6	1.2	35.2	1.5	7.5	25.5	11.8	106.0
2	-1.08	0	-2.92	49.1	17.9	17.9	2.6	3.9	9.5	4.1	107.0
3	-1.09	10	-1.87	18.3	0.1	39.8	0.7	7.3	26.7	11.3	106.2
4	-1.06	0	-4.73	46.1	13.6	16.9	2.0	5.5	7.3	3.0	95.9

Entry 1: electrolysis with 10 mM N-tolyl pyridinium in 0.1 M $KHCO_{3(aq)}$.
Entry 2: film formed during electrolysis entry 1 wiped off surface, and electrolyte replace with 0.1 M $KHCO_{3(aq)}$.
Entry 3: electrolysis with 10 mM N-tolyl pyridinium in 0.1 M $KHCO_{3(aq)}$.
Entry 4: film formed during electrolysis entry 1 dissolved in acetone, but kept on electrode, subsequently dried, and electrolyte replace with 0.1 M $KHCO_{3(aq)}$.

Table S8. Faradaic efficiency (%) towards different products produced during CO_2 reduction on a polycrystalline copper electrode in a CO_2 saturated 0.1 M $KHCO_3$ electrolyte with different compounds at an applied potential of -1.1 V vs. RHE. Experiments with multiple runs are listed.

Compound	Faradaic Efficiencies (%)										
	CH_4	C_2H_4	C_2H_5OH	C_3H_7OH	CO	H_2	$HCOO^-$	$C_{\geq 2}$	Total	$C_{\geq 2}/CH_4$	j (mA/cm^2)
None	22.0	15.8	8.2	3.2	1.1	36.4	3.4	29.7	92.6	1.1	-5.02
	14.0	11.1	7.6	2.7	2.9	49.4	5.5	25.2	97.1	1.1	-4.15
	24.7	10.1	5.9	2.6	1.1	42.5	5.3	23.0	96.6	0.7	-4.21
1	2.1	36.4	29.8	9.4	1.4	15.9	7.2	75.5	102.1	36	-0.99
	0.6	41.0	28.3	4.3	3.6	17.7	6.2	73.6	102.0	122	-0.93
	0.3	44.2	33.7	7.5	0.5	12.9	6.2	85.4	105.3	285	-1.15
1-d_5	0.1	37.6	26.5	8.6	2.4	24.4	5.4	72.7	105.0	727	-0.80
3	2.6	31.0	32.6	0	1.3	19.8	8.8	63.6	95.8	24	-0.75
	3.6	27.5	26.6	0	3.6	23.8	11.3	54.1	96.4	15	-0.64
4	0.13	36.0	25.5	9.9	2.6	14.3	12.9	71.4	101.0	549	-1.47
	0.5	39.4	19.0	7.4	1.5	19.1	8.3	65.8	95.5	132	-1.44
5	0.05	41.2	24.3	8.7	2.4	11.4	8.6	74.2	98.3	1484	-1.36
	0.17	40.3	29.1	8.5	1.7	13.3	8.9	77.9	102.0	458	-1.32
6	3.3	15.7	13.5	0	5.6	50.1	7.3	29.2	98.9	9	-1.46
	0.9	20.7	18.5	0	1.8	54.0	6.5	39.2	102.0	44	-1.34
7	0.09	31.9	29.7	13.5	3.5	10.6	13.2	75.1	102.0	834	-1.02
	0.05	35.2	24.4	10.0	2.7	9.4	12.8	69.6	96.5	1392	-1.17
8	6.9	0.8	0	2.9	2.7	60.0	11.0	3.7	84.4	0.5	-3.33
	3.2	2.6	0	7.6	2.4	49.0	10.2	10.2	74.7	3.2	-3.31
9	0.3	0.06	0	2.1	0.4	88.0	5.7	2.16	97.0		-6.23
	0.5	0.05	0	2.1	0.3	89.0	5.5	2.15	98.0		-6.33
10	0.02	0	0	0	0.2	65.9	9.3	0	70.8		-3.10
	0.06	0	0	0	0.2	70.5	9.7	0	80.5		-2.80
11	0	3.0	0	0	0.9	26.6	10.5	3.2	41.0		-0.94
	0	3.4	0	0	0.5	30.6	7.5	3.4	42.0		-1.00
12	5.2	3.5	0	0	0.3	60.2	6.5	3.5	75.7		-4.10
	3.2	4.5	0	0	0.3	63.0	4.5	4.5	75.2		-3.95
13	0.01	0.05	0	0	0.2	73.0	2.0	0.05	75.3		-7.10
	0.01	0.09	0	0	0.8	80.2	0.6	0.09	81.7		-5.77
14	0.07	0.0	0	0	0.03	94.4	1.9	0	96.4		-3.94
	0.4	0.02	0	0	0.5	88.1	8.7	0.02	97.7		-4.45
9 + toluene	0.6	0.4	0	2.3	1.3	80.0	9.0	2.7	93.6		-6.74
9 + 4-methylphenyl	1.0	0.3	0	2.0	0.3	90.0	6.2	2.3	99.8		-7.68
4-methylphenyl	31	19	5.9	3.3	1.3	36	4.5	28.2	102		-4.69
2 (0.5 mg) (dropcast in tol)	7.1	2.2	0	0	1.5	77.7	6.5	2.2	94.0		-4.10
2 (4.2 mg) (dropcast in DCM)	0.3	0.2	0	0	1.4	90.7	6.7	0.2	99.3		-2.99

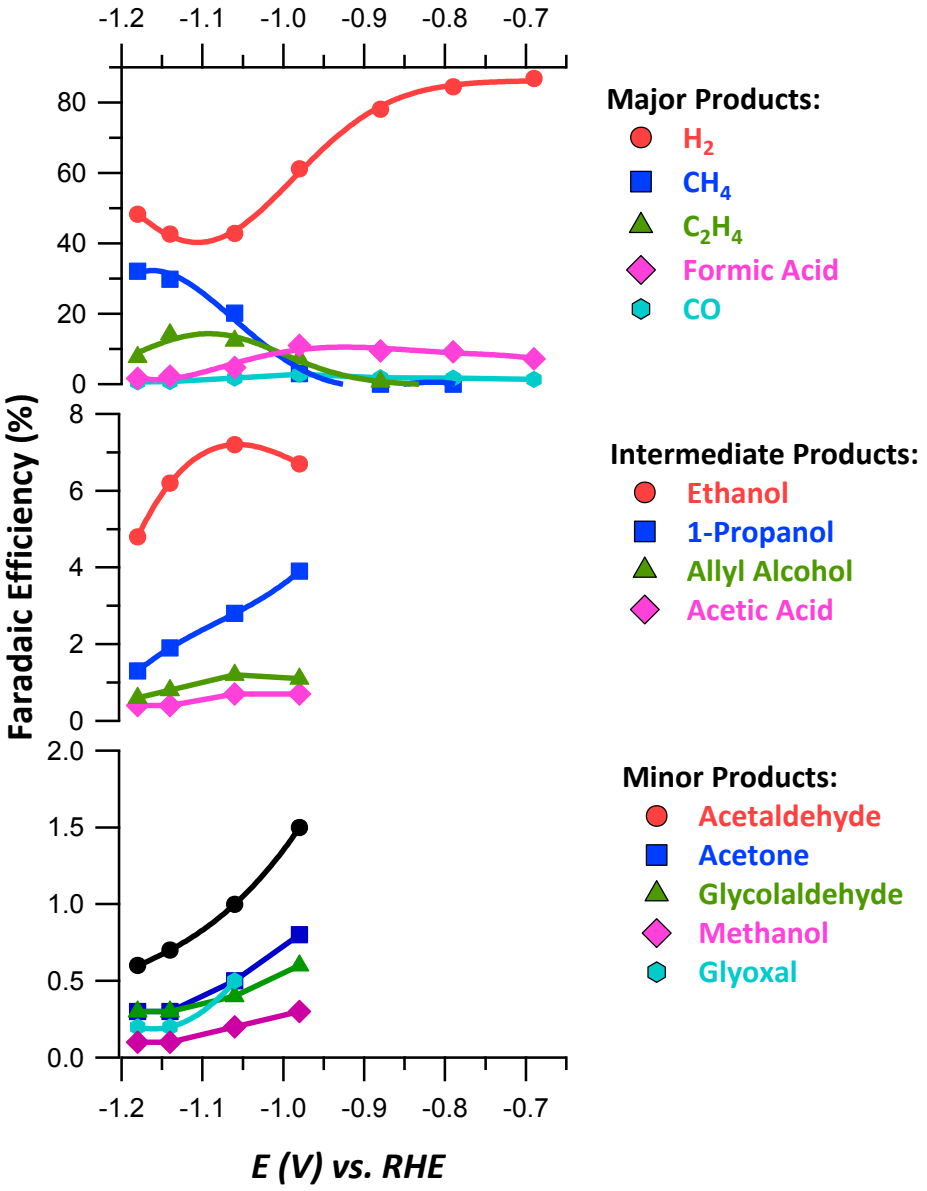

Figure S17. Faradaic efficiency towards different products produced during CO_2 reduction on a polycrystalline copper electrode in a CO_2 saturated 0.1 M $KHCO_3$ electrolyte at different applied potentials.

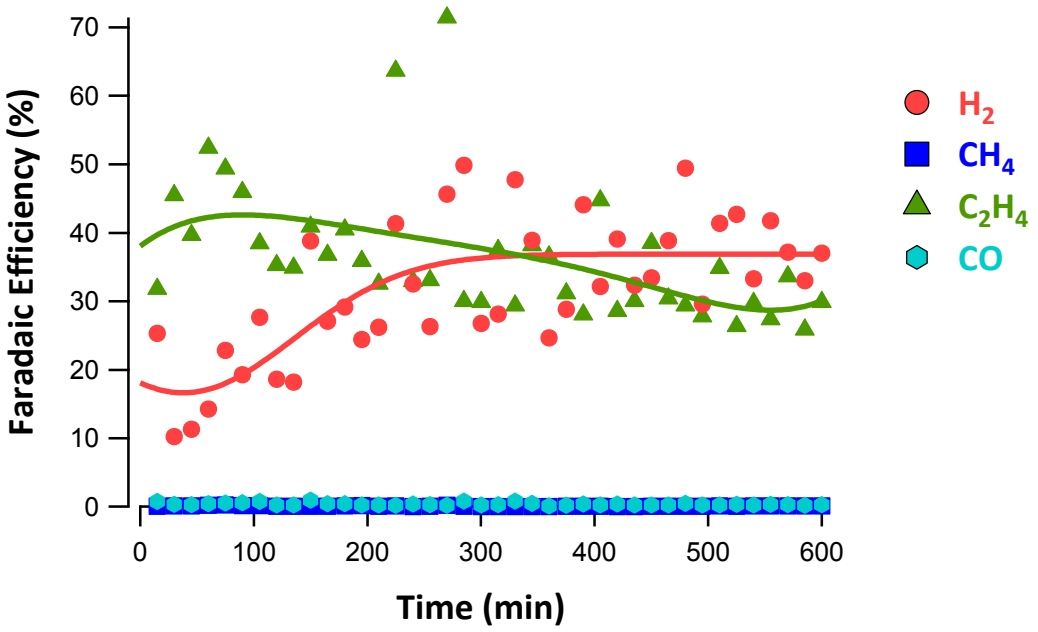

Figure S18. Faradaic efficiency towards gaseous products produced during long term CO_2 reduction for 10 hours on a polycrystalline copper electrode in a CO_2 saturated 0.1 M $KHCO_3$ electrolyte with 10 mM N-tolyl pyridinium (1).

S8. XPS spectra

X-ray photoelectron spectroscopy (XPS) data were collected using a Surface Science Instruments M-Probe ESCA controlled by Hawk Data Collection software (Service Physics, Bend OR; V7.04.04). The monochromatic X-ray source was the Al K_α line at 1486.6 eV, directed at 35° to the sample surface (55° off normal). Emitted photoelectrons were collected at an angle of 35° with respect to the sample surface (55° off normal) by a hemispherical analyzer. The angle between the electron collection lens and X-ray source is 71°. Low-resolution survey spectra were acquired between binding energies of 1-1000 eV. Higher-resolution detailed scans, with a resolution of ~0.8 eV, were collected on individual XPS lines of interest. The sample chamber was maintained at $< 2 \times 10^{-9}$ Torr. The XPS data were analyzed using the CasaXPS software. Copper foils after electropolishing or electrolysis were rinsed with copious amount of water, dried under a stream of nitrogen and immediately transferred to a nitrogen glove box before XPS measurements. For the copper foil after electrolysis in the presence of **1**, the electrode surface was further rinsed with hexanes (~15 mL) to remove the precipitates in the glove box.

XPS spectra suggest that the surfaces of copper foils are mixtures of copper metal and Cu_2O, for the electropolished surfaces before and after electrolysis with and without 10 mM of **1**. For the sample after electrolysis in the presence of **1**, residual of **2** is observed after rinsing with hexanes. Due to the complexity of the organic molecule in the C 1s region, spectral energy for all samples are calibrated using the Cu $2p_{3/2}$ peak (932.63 eV) instead of C 1s. The Cu 2p band for all three samples shows a pair of narrow (fwhm $\approx$ 1.4 eV) $2p_{3/2}$ and $2p_{1/2}$ peaks, indicative of Cu metal and/or Cu_2O. These two oxidation states in the 2p region give near identical binding energy. These peaks fit nicely employing Gaussian (20%)- Lorentzian (80%) lineshape.[6] The lack of large satellites at 940–945 and 960–963 eV indicates that the surfaces do not contain CuO. Cu Auger electron (LMM) band for each sample shows a sharp peak at 918.5 eV and a smaller peak at 916.5 eV, which are characteristics of copper metal and Cu_2O, respectively. For the sample after electrolysis in the presence of **1**, a N 1s peak is observed at 400.6 eV, which is smaller than pyridinium (~402.5 eV) and similar to a tertiary amine. (400.2 eV).[7-8] This observation is consistent with the ^{1}H NMR and crystallography for the assignment of the precipitate to be **2**.

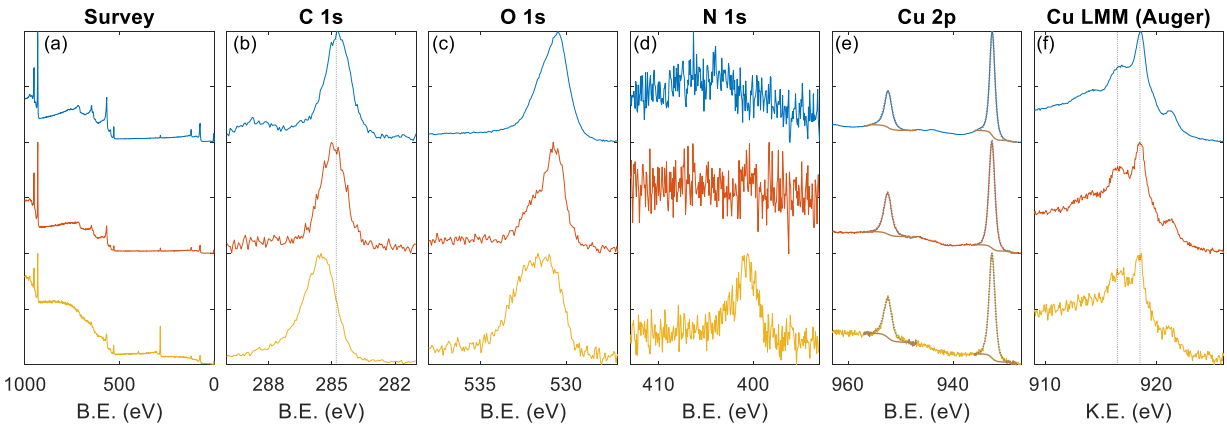

Figure S19. Normalized (a-e) X-ray photoelectron and (f) Auger electron spectra of electropolished Cu foil before electrolysis (top) and after electrolysis at -1.09 V vs RHE in $KHCO_{3(aq)}$ (0.1 M) without (middle) and with (bottom) **1** (10 mM) in the catholyte solution. Dotted line in (e) is the fit. B.E. is electron binding energy and K.E. is electron kinetic energy. Vertical dashed lines in (b): 284.8 eV (adventitious carbon) and in (f): 916.5 and 918.5 eV.

S9. Additional GC-MS and NMR data of gas and liquid products

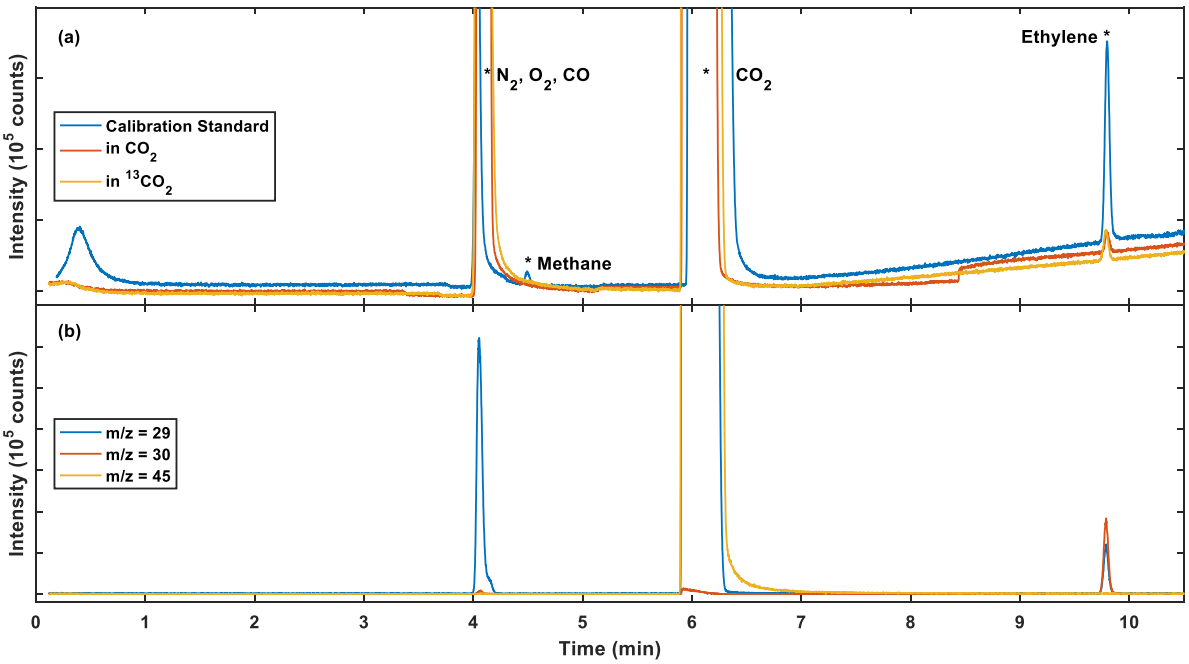

Figure S20. Additional GC-MS data for Figure 3a. (a) GC-MS total ion chromatograms of calibration standard and gas products from bulk electrolysis at -1.09 V vs RHE in **1** (10 mM) and natural abundance and ^{13}C-enriched CO_2-saturated $KHCO_3$ (0.1 M). (b) Extracted ion chromatogram of selected m/z from ^{13}C experiment.

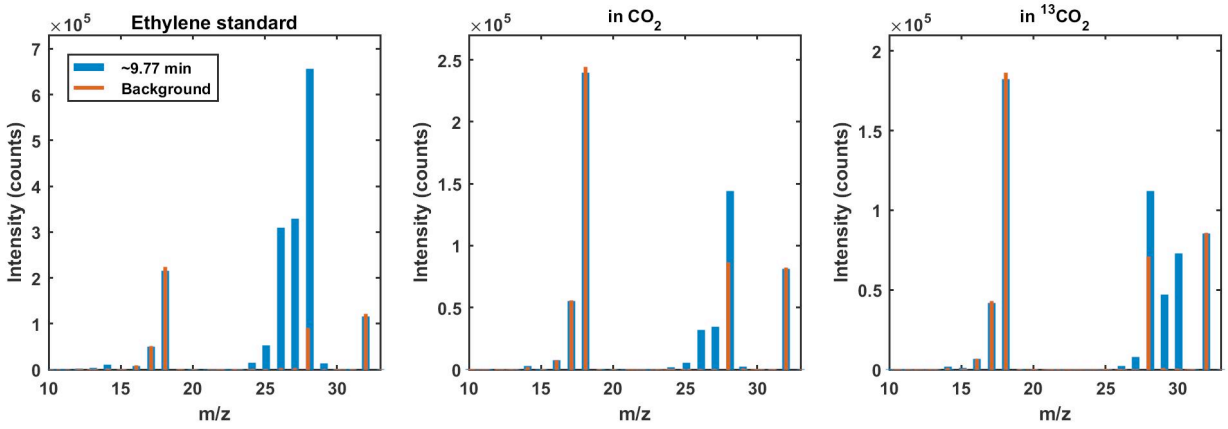

Figure S21. Raw GC-MS spectra shown in Figure 3a.

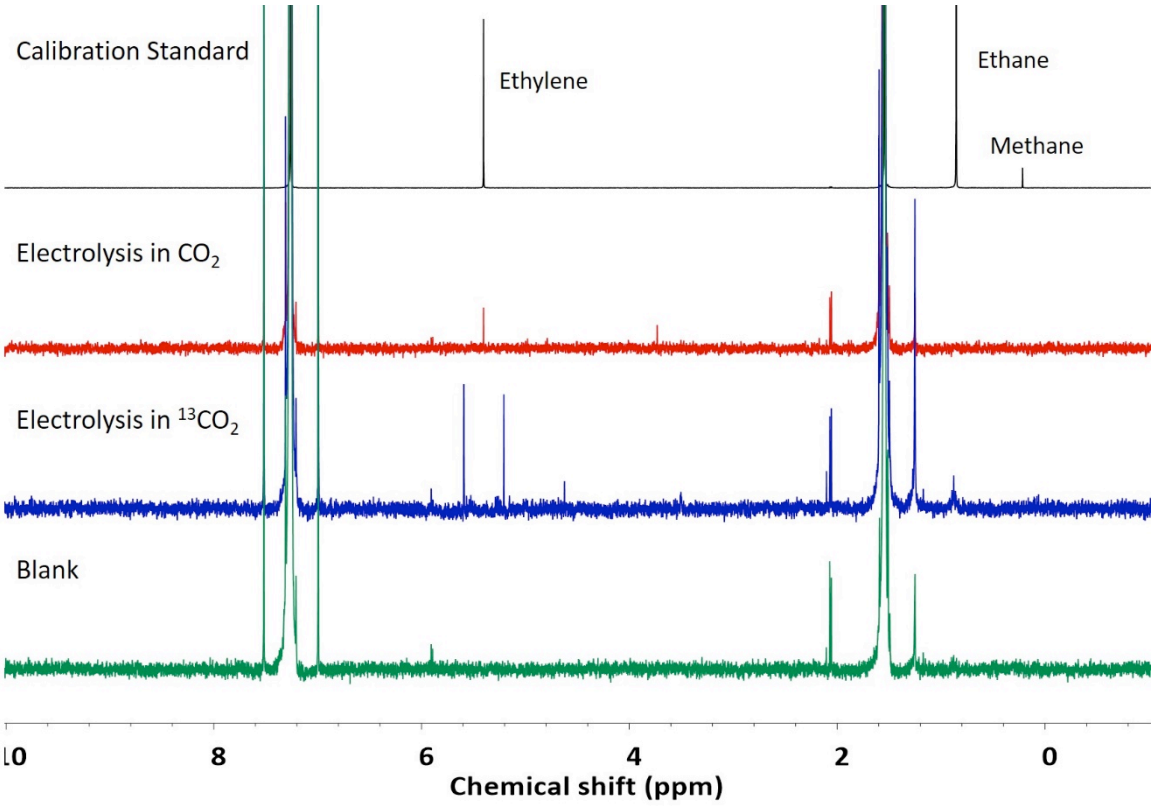

Figure S22. Full ^{1}H NMR spectra (400 MHz, $CDCl_3$) shown in Figure 3b: Natural abundant calibration standard purchased from Airgas (black) and gas product after bulk electrolysis at -1.09 V vs RHE in **1** (10 mM) and natural abundance (red) and ^{13}C-enriched (blue) CO_2-saturated $KHCO_3$ (0.1 M).

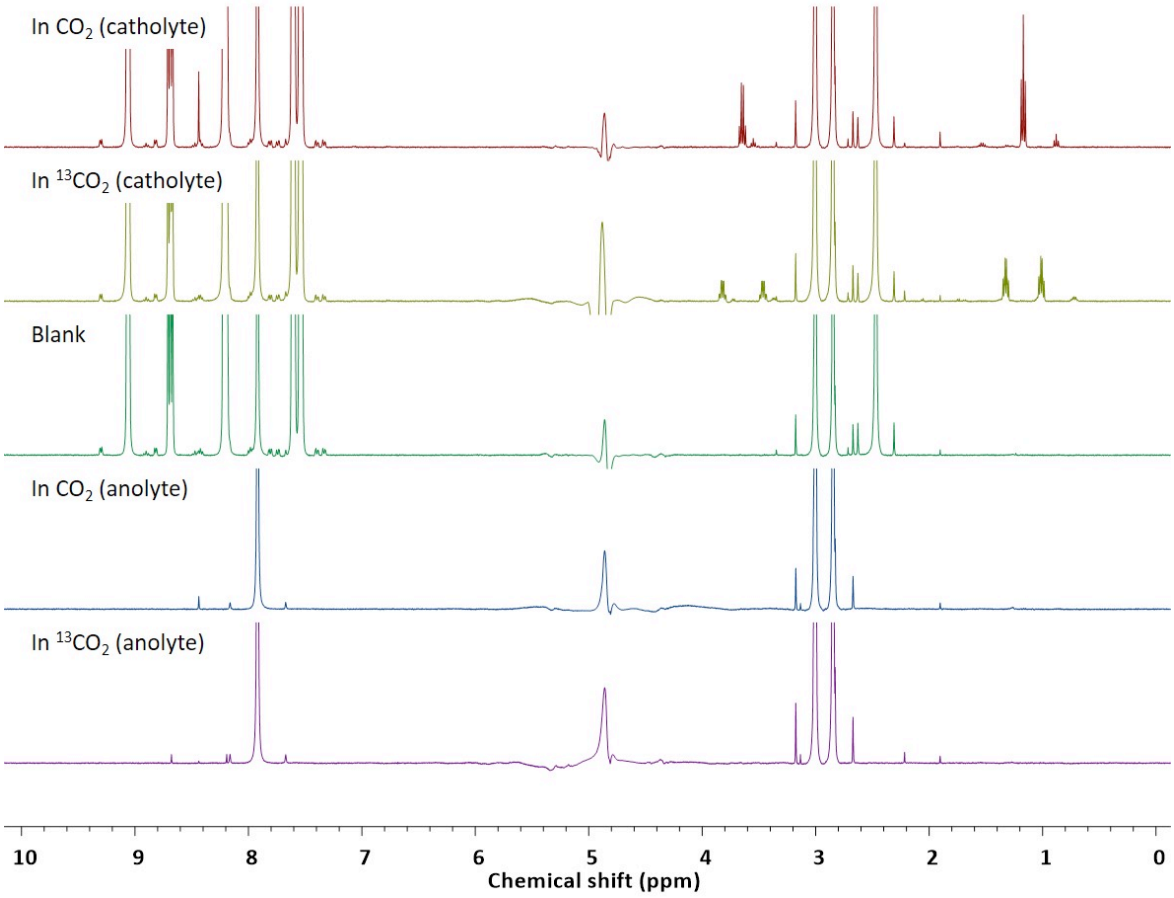

Figure S23. Full ^{1}H NMR spectra (400 MHz, H_2O:D_2O = 9:1) of the catholytes and anolytes after bulk electrolysis at -1.09 V vs RHE in **1** (10 mM) and natural abundance and ^{13}C-enriched CO_2-saturated $KHCO_3$ (0.1 M). shown in Figure 3c. Spectrum of electrolyte before electrolysis (blank) is also included.

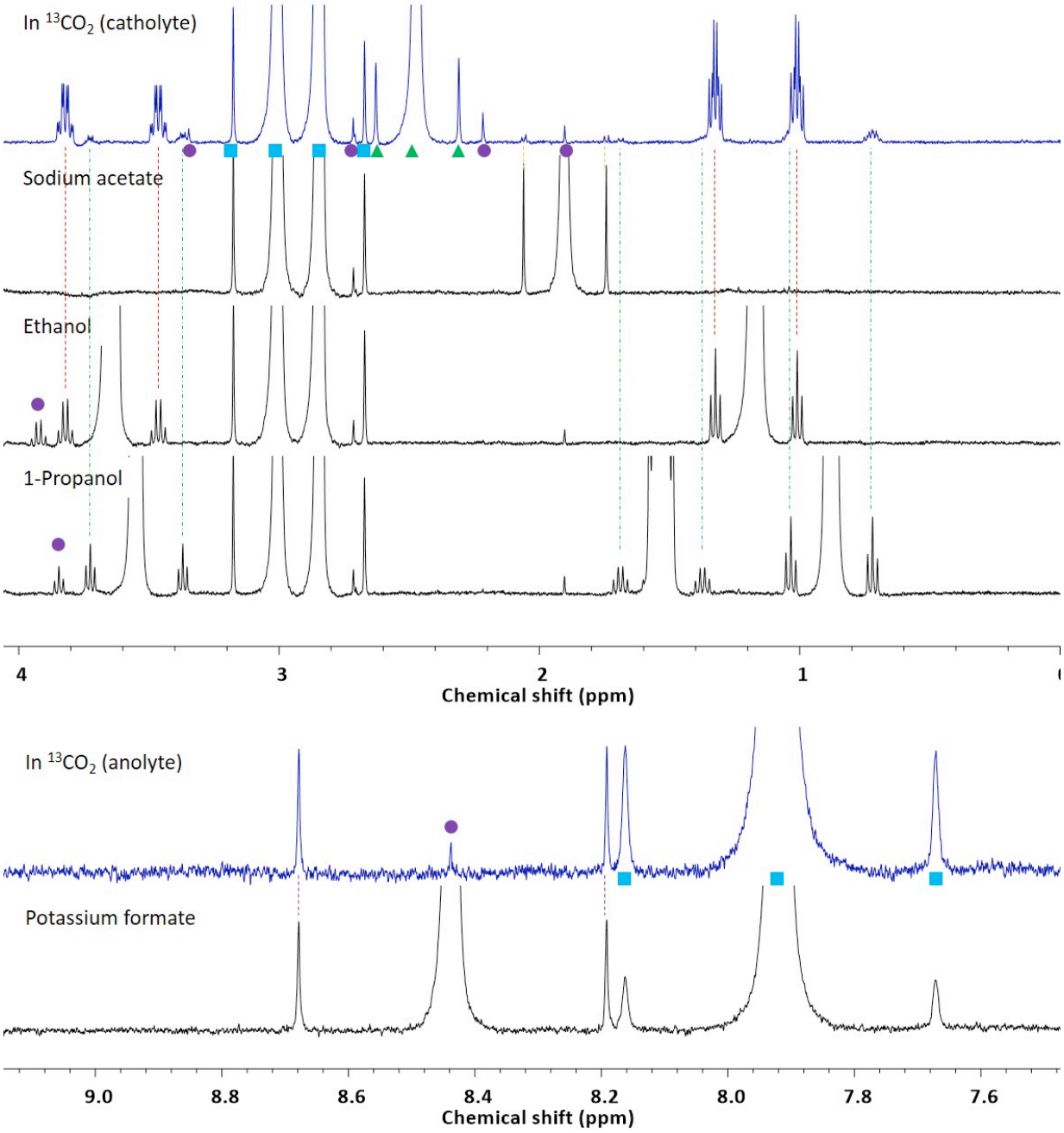

Figure S24. (Blue) ^{1}H NMR spectra (400 MHz, 90% H_2O/10% D_2O (v/v)) of catholyte and anolyte after bulk electrolysis at -1.09 V vs RHE in **1** (10 mM) and natural abundance (red) and ^{13}C-enriched (blue) CO_2-saturated $KHCO_3$ (0.1 M). The $^{1}J_{CH}$ of each product matches with the ^{13}C satellites of the corresponding compound (Black). Square: DMF (Internal standard, 12.9 mM). Triangle: **1**. Round: Other impurities.

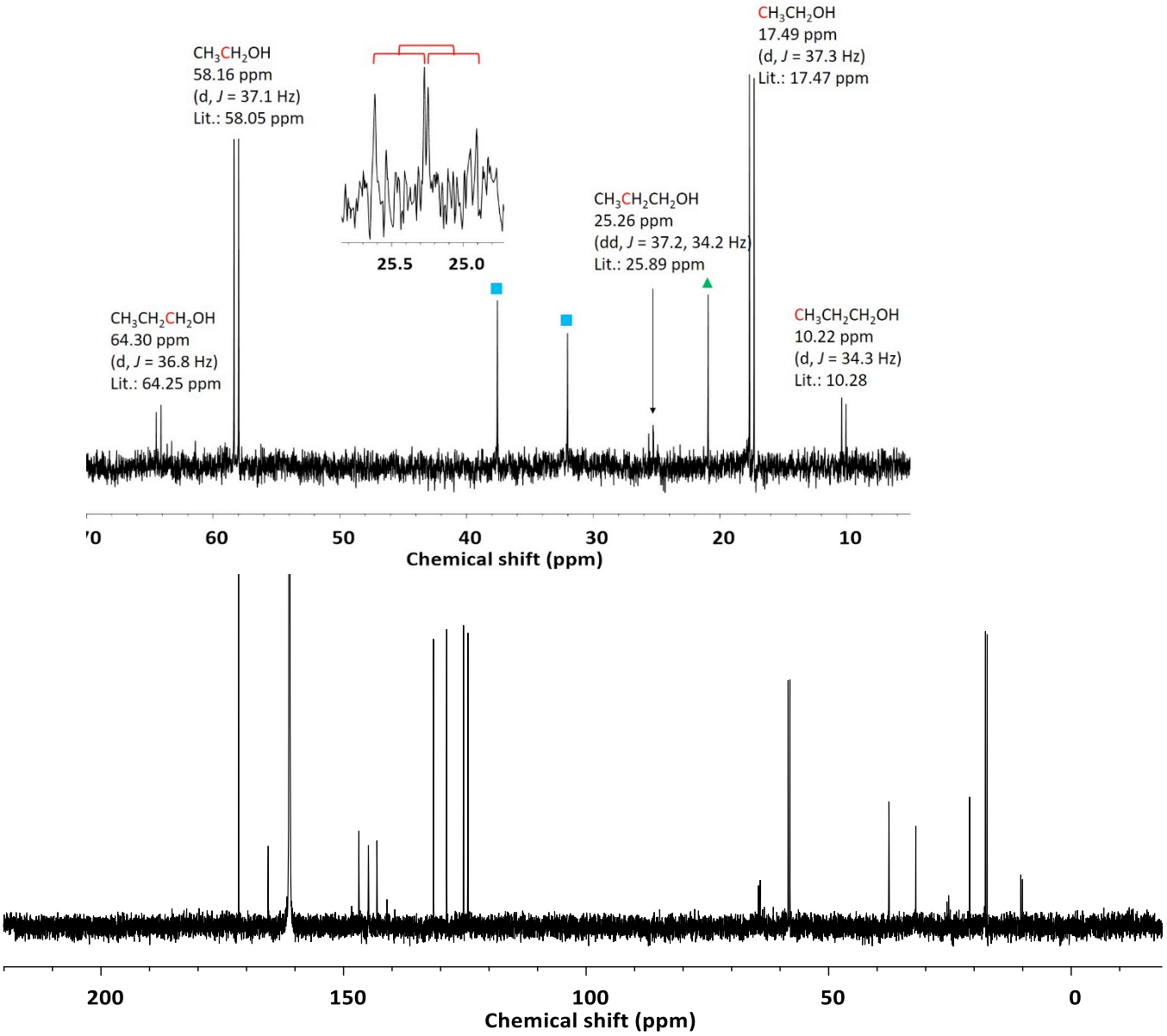

Figure S25. (Top) ^{13}C NMR spectrum (101 MHz, H_2O:D_2O = 9:1) of catholyte after bulk electrolysis at -1.09 V vs RHE with **1** (10 mM, triangle) and ^{13}C-enriched 0.1 M of $KHCO_{3(aq)}$ and CO_2. Internal standard: DMF (CH, 165.53 ppm, square). (Bottom) Full spectrum of the same measurement**.**

S10. X-ray crystallography

Suitable crystals were mounted on a nylon loop using Paratone oil, then placed on a diffractometer under a nitrogen stream. X-ray intensity data were collected on a Bruker D8 VENTURE Kappa Duo PHOTON 100 CMOS detector employing Mo-Kα radiation (λ = 0.71073 Å) at a temperature of 100 K. All diffractometer manipulations, including data collection, integration and scaling were carried out using the Bruker APEX3 software. Frames were integrated using SAINT. The intensity data were corrected for Lorentz and polarization effects and for absorption using SADABS. Space groups were determined on the basis of systematic absences and intensity statistics using XPREP. Using Olex2,[9] the structures were solved using ShelXT and refined to convergence by full-matrix least squares minimization using ShelXL. All non-solvent non-hydrogen atoms were refined using anisotropic displacement parameters. Hydrogen atoms were placed in idealized positions and refined using a riding model. Graphical representation of structures with 50% probability thermal ellipsoids was generated using Diamond and Mercury visualization software.

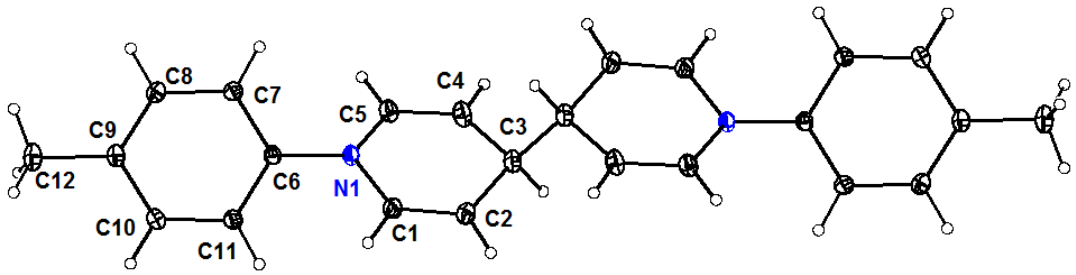

Figure S26. ORTEP diagram of 1,1'-ditolyl-4.4'-dihydro-4.4'-bipyridine (**2**) at 50% probability.

Table S9. Crystal data and structure refinement for 1,1'-ditolyl-4.4'-dihydro-4.4'-bipyridine (**2**).

Compound	**2**
CCDC	1556377
Empirical formula	$C_{24}H_{24}N_2$
Formula weight	340.47
Temperature/K	99.97
Crystal system	triclinic
Space group	P-1
a/Å	9.2368(6)
b/Å	9.60549(6)
c/Å	11.1978(8)
α/°	97.319(1)
β/°	103.470(2)
γ/°	108.113(2)
Volume/Å^3	896.58(10)
Z	2
ρ_{calc}g/cm^3	1.246
μ/mm^{-1}	0.073
F(000)	356.0
Crystal size/mm^3	0.39 × 0.16 × 0.05
Radiation	MoKα (λ = 0.71073)
2Θ range for data collection/°	4.57 to 75.21
Index ranges	-15 ≤ h ≤ 15, -15 ≤ k ≤ 16, -18 ≤ l ≤ 18
Reflections collected	27294
Independent reflections	8820 [R_{int} = 0.0287, R_{sigma} = 0.0380]
Data/restraints/parameters	8820/0/237
Goodness-of-fit on F^2	1.027
Final R indexes [I>=2σ (I)]	R_1 = 0.0522, wR_2 = 0.1355
Final R indexes [all data]	R_1 = 0.0770, wR_2 = 0.1501
Largest diff. peak/hole / e Å^{-3}	0.60/-0.38

References

1. Zeghbib, N.; Thelliere, P.; Rivard, M.; Martens, T. *J. Org. Chem.* **2016**, *81*,3256−3262
2. Hong, A. Y.; Vanderwal, C. D. *J. Am. Chem. Soc.*, **2015**, *137*, 7306–7309
3. Eda, M.; Kurth, M. J.; Nantz, M. H. *J. Org. Chem.* **2000,** *65,* 5131–5135
4. Kuhl, K.P.; Cave, E.R.; Abram, D.N.; Jaramillo, T.F. *Energy Environ. Sci.* **2012**, *5*, 7050–7059.
5. Lobaccaro, P.; Singh, M.R.; Clark, E.L.; Kwon, Y.; Bell, A.T.; Ager, J.W. *Phys. Chem. Chem. Phys.*, **2016**, *18*, 26777–26785.
6. Biesinger, M.C.; Lau, L.W.M.; Gerson, A.R.; Smart, R.St.C. *Appl. Surf. Sci*, **2010**, *257*, 887–898.
7. Men, S.; Mitchell, D.S.; Lovelock, K.R.J.; Licence, P. *ChemPhysChem*, **2015**, *16*, 2211–2218.
8. Zhao, Y.; Liu, X.; Han, Y. *RSC Adv.*, **2015**, *5*, 30310–30330.
9. Dolomanov, O.V.; Bourhis, L.J.; Gildea, R.J.; Howard, J.A.K.; Puschmann, H., OLEX2: A complete structure solution, refinement and analysis program (2009). J. Appl. Cryst., *42*, 339.